FLOW STRUCTURE IN THE HORIZONTAL SLUG FLOW

E. S. Rosa

Universidade Estadual de Campinas
Faculdade de Engenharia Mecânica
Departamento de Energia
CP 6122
CP. 13083-970, Campinas, SP, Brasil
erosa@fem.unicamp.br

ABSTRACT

Successions of long gas bubbles and liquid slugs form the so-called slug flow pattern in a gas-liquid flow. A unit cell encompassing one gas bubble and one liquid slug characterizes this alternating gas-liquid flow. The kinematic and dynamic flow mechanisms responsible for the interactions between the successive unit cells are still an open question. Inside this context, this work addresses specifically to the bubble velocity, the bubble to bubble interactions and the entrance mechanisms. Within an experimental framework the spatial evolution of each unit cell structure is individualized during the acquisition period. The experimental apparatus consisted of a 23.4 m long transparent Plexiglas pipe, 26mm ID, which means a total relative length of 900 free diameters. The air and water were mixed at the inlet of the test section and discharged into a collecting tank open to the atmosphere. The instantaneous measurements of the flow structure were made with double-wire conductive probes. The probes were installed in four measuring stations; each station had two probes slightly apart. The measuring stations were located at 127D, 273D, 506D e 777D from the mixer. The experimental database is further processed to give rise to histograms and correlations among flow variables

Keywords: slug flow, bubble velocity, drift velocity, horizontal, two-phase flow

NOMENCLATURE

A cross section pipe area, m^2
BF bubble front time detected by front sensor, s
BR bubble front time detected by rear sensor, s
C_0 phase distribution parameter
D pipe internal diameter, m
J mixture superficial velocity, m/s
JL liquid superficial velocity, m/s
JG gas superficial velocity, m/s
LB bubble length, m
LS liquid slug length, m
Fr Froude number, $J/(gd)^{0.5}$
R correlation coefficient
Re Reynolds number, Jd/ν
S standard deviation
s probe spacing, m
SF slug front time detected by front sensor, s
SR slug front time detected by rear sensor, s
T unit cell period, s
VB front bubble velocity, m/s
VS front slug velocity, m/s
<x> average operator of a generic variable x

Greek symbols

α void fraction
ρ density, kg/m^3
ν liquid kinematic viscosity, m^2/s

INTRODUCTION

Still today the so-called "unit cell" is the most used mechanistic representation of the gas-liquid slug flow. The concept, originally proposed by Dukler and Hubbard (1975), divides the flow in two structures. One is the liquid slug, which carries primarily liquid and some dispersed gas, in a typical dispersed bubbly flow pattern; the other is formed by an elongated gas bubble flowing over a liquid film. The structures occur successively in the pipe as the mixture flows and compose the unit cell, as shown in Fig. 1.

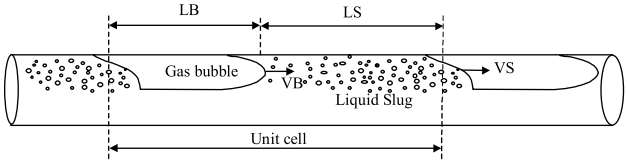

Figure 1. The unit cell and the mechanistic representation of slug flows.

To model the flow according to this concept, one generally uses the one-dimensional time and spaced averaged mass and momentum equations, complemented by constitutive relations. The conservation equations are written for inertial control volumes, one fixed and the other displacing

at the velocity of the unit cell. The velocity of the unit cell is assumed to be unique, which requires the mixture flowing as a succession of identical unit cells traveling at constant velocity. Using the approach outlined it is possible to predict the averaged length of the structures, the pressure drop, the liquid hold-up and the averaged heat transfer coefficient, among other physical parameters of interest. This was, in some way, what Bendiksen (1984), Barnea and Brauner (1985), Dukler et al. (1985), Andreussi and Bendiksen (1989), Barnea and Taitel (1993) did.

Slug flow models based on the unit cell concept are relatively easy to implement. They give reliable results of average pressure and flow rates and its use is wide spread in flow simulators. The correctness of the predictions, as usual, will reflect the simplifications and the proper use of the constitutive equations that provide the closure. One major shortcoming is intrinsic to the above mentioned assumption, i.e., that *identical cells travels at constant velocity;* other refers to the constitutive equations, usually revealed by the analysis of experimental data obtained with *fully developed slug flows*. The first assumption does not attend the main characteristic of the slug flow pattern: the intermittence and irregularity. The second assumption does not consider the frequency and sizes at the section where the slugs are formed (entrance mechanism) and their evolution by coalescence (overtaking mechanism) but assumes the gas-liquid structures evolving to a stationary unit size and frequency.

A better representation of the flow would result if the information on the non-uniformity of length and velocity present on a train of elongated bubbles and liquid slugs were considered. Likewise, the results would be more precise if the model could take into account the changes that the unit cells undergo as they advance in the pipe. These changes result from the interactions between successive cells, which are particularly intense up to some distance down-stream the mixer but still remains at locations far from it due to the continuous expansion of the gas. Thus, rigorously, it is not expected to achieve a space and time periodic behavior in this flow, which could be referred as a fully developed slug flow.

The kinematic and dynamical behavior of the slug flow has been experimentally investigated using statistical analysis. The histograms of the sizes and velocities downstream of the mixer arise in the work of Nydal et al. (1991) and Grenier (1997). These authors performed experiments with air/water flows in horizontal pipelines with 53 mm and 90 mm ID, respectively. Their test sections were at 312D and 1698D far from the gas-liquid mixer, in this order. More recently, Rosa et al. (2001 a-b) presents data on the evolution air-water slug flows in a 26 mm ID horizontal pipeline that is 900 relative diameters long. It complements the previous works in the sense that discloses experimental data taken by eight probes installed in four measuring stations located at different distances from the air-water mixer, every station having a pair of probes mounted 50 mm apart. Moreover, it reveals data on the evolution of the structures that form the unit cells as they flow along the pipe. The results include the statistical analysis and respective comparisons of the velocity and length of the elongated bubble and the aerated slug, the frequency of the unit cell and the coalescence rate. The present work further extend the previous analysis in Rosa et al. (2001 a-b) investigating experimentally the bubble velocity, the interactions between consecutive bubbles and the role of the entrance mechanism on the formation and evolution of the slug structures.

EXPERIMENTAL SET-UP

A sketch of the experimental set-up appears in Figure 2. It includes a horizontal pipeline, storage and receiving tanks mixers, control valves, pumps, compressors and instrumentation. The test section is a 26 mm ID straight transparent Plexiglas pipeline 900 pipe diameters long, i.e., 23.4 m. The working fluids were ordinary tap water and compressed air. High capacity compressors and a centrifugal pump supply the air and the water to the mixer installed at the entrance of the test section. Two different mixers have been used in order to detect the influence of the mixing process on the formation and evolution of the slug flow. The first mixer was made of two concentric tubes, here after called by concentric stream mixer, CSM. The inner tube delivers the air through a small orifice while the water flows trough the annular space. The second mixer was made of a single tube with a Plexiglas sheet dividing its cross section in two separated channels, also called by parallel stream mixer, PSM. Two parallel streams of water and air are formed inside the mixer and put together at the outlet. The use of CSM or PSM is to observe the

differences on the flow structures at the slug formation processes and how these structures evolve along the pipe. At the other end of the test section the mixture is discharged, without restraint, into a receiving tank open to the atmosphere (in average, 0.94 bar and 25°C). From the receiving tank the water is transferred to the main tank, so that the total volume contained by the system adds-up to 3 m^3, ensuring a fairly constant water temperature during the experiment.

The water flow-rate was measured by a set of two orifice plates that were calibrated at 1½% of monitored uncertainty. To measure the air flow-rate one used two Merian© laminar flow elements with reported an uncertainty of 1%. The range of air superficial velocities varied between 0.4 Sm/s to 1.7 Sm/s. The water superficial velocities ranged from 0.25 m/s to 1.35 m/s. The letter S in front of the unit specify the local atmospheric condition (0.947 bar @ 21°C); otherwise it refers to the *in situ* conditions.

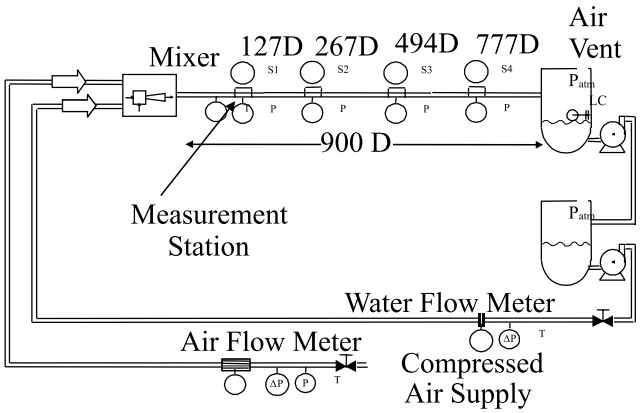

Figure 2. Schematics of the experimental set up.

The gas and liquid flow rates as well as the temperature and pressure were continuously monitored, controlled and registered by a data acquisition system.

The gas-liquid flow structures are detected by four measuring stations distributed along the pipeline, S1 to S4 in Fig. 2. In every measuring station there is installed a pair of double-wire probes, 50 mm apart, and a pressure transducer. The later measures the flow pressure drop. The former are double cross section wire conductive probe which, detecting the passage of bubble and liquid slug fronts, renders theirs propagation velocity, the frequency, the length and the coalescence rate, as they evolve along the pipeline.

Typical signals, taken simultaneously by the twin probes appear shifted in time in Fig. 3. The liquid film flows bellow or, sometimes, surrounding the elongated bubble, and creates the low-level signal. The liquid slug produces the high level signal. This time-based signal discriminates the gas-liquid structures that compose the unit cells.

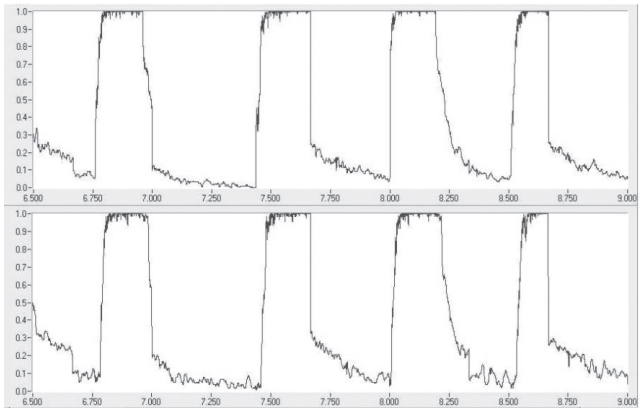

Figure 3. The time signals delivered by the double-wire probes mounted in a measuring station, amplitude (V) versus time (s), grabbed from the computer screen.

The probe driving circuit, the sampling frequency and further treatment of the raw data are described in Rosa et al. (2001 a-b) and will not be reproduced here. Even tough is necessary to say that the voltage signal is transformed in a sequence of square waves with minimum and maximum of 0 and 1 by applying a cut-off voltage. Voltages values above the cut-off value became (1) otherwise (0) and are associated with the occurrence of the liquid slug or the elongated bubble, respectively. Figure 4 shows a representative sample of the square wave signals, obtained after applying a proper threshold level to the original voltage signals.

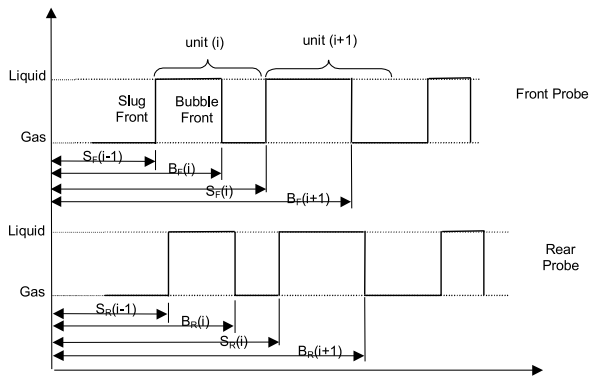

Figure 4. A pair of square-wave signals identifying the structures of the slug and bubble fronts.

The resistive probes measure the time of liquid and gas events inside the pipe from an Eulerian frame of reference. Taking for reference Fig. 4, the wave in the upper part is from the front sensor, while the one in the lower part is from the rear sensor. The i^{th} liquid slug trailed by the i^{th}-elongated bubble composes the i^{th} unit cell. B(i) and S(i) specifies the time of occurrence of the bubble front and the slug front, respectively. The subscript $_{(F)}$ and $_{(R)}$ refers to the front or rear probe, convention established in regards the flow direction. The values of the unit period, and the velocities of the bubble and slug fronts are determined using the time records of the twin probes. The period of the i^{th} unit cell is evaluated as:

$$T(i)=S_F(i)-S_F(i-1) \tag{1}$$

The bubble front velocity, VB(i) is estimated as the ratio of the probe spacing (s = 50mm) and the time delay between the front and rear sensor events:

$$VB(i) = s/[B_R(i) - B_F(i)] \tag{2}$$

The bubble and slug lengths are defined by their time ratio expressed by the velocity difference between their front and tail, Eqs. (3) and (4). While VB and VS are the instantaneous velocity of the bubble and slug front, the same does not apply to the length estimates. The difficulty arises because for length determinations are necessary velocities measurements following the bubble or the slug, i.e., in a Lagrangian frame of reference as well as an initial length to start with the integration procedures of Eqs. (3) and (4). Furthermore, the recorded velocities either from the i^{th} bubble front or to the slug front are delayed in time owing to the length of the bubble, which is typically several pipe diameters long. Therefore instantaneous front and tail velocities are never known at the same instant because the probes are stationary.

$$\frac{d}{dt}LB(i) = VB(i+1) - VS(i), \tag{3}$$

and,

$$\frac{d}{dt}LS(i) = VS(i) - VB(i) \tag{4}$$

Focusing on the bubble, these experimental difficulties are overcome considering that the gas is transported within the bubble. Therefore its volume V is related to its length by its void fraction α times the pipe area cross section A,

$$V = LB \cdot A \cdot \alpha \tag{5}$$

Taking the time derivative of Eq. (5) and using the ideal gas law one gets:

$$\frac{dLB}{dt} = \frac{LB}{P} \cdot VB \cdot \frac{dP}{dx} \tag{6}$$

considering dP/dt = VB.(dP/dx). Estimates of Eq.(6) for the given experimental conditions shows that dLB/dt ranges between 0.0001 to 0.01 m/s for all runs. This experimental result gives support to state that in average the bubble and slug front have the same velocities, and the integration of Eq. (3) simplifies to:

$$LB(i) = VB(i) \cdot [S_F(i) - B_F(i)] \tag{7}$$

The same straightforward analysis for the slug length can not be applied because the liquid is transported by the slug as well as by the film underneath the bubble. But since the bubble front and bubble tail have approximately the same velocities it is assumed that the slug length can be estimated by

$$LS(i) = VB(i) \cdot [B_F(i) - S_F(i-1)] \tag{8}$$

which is an Euler forward first order approximation.

The outcome of post-processing the experimental data is an array representing the velocity, length and period of every elongated bubble and liquid slug that passed by the sensors. It is then further processed statistically, giving rise to average values, standard deviations, histograms and correlation coefficients. From here on, for sake of conciseness, the average value of a generic discrete variable x will appear as <x>, the standard deviation as Sx and the correlation coefficient Rxy. They are evaluated as:

$$\langle x \rangle = \frac{1}{N}\sum_{i=1}^{N} x_i \tag{9}$$

$$S_x = \sqrt{\frac{1}{N-1}\sum_{i=1}^{N}\left[\langle x\rangle - x_i\right]^2} \qquad (10)$$

$$R_{xy} = \frac{\frac{1}{N-1}\sum_{i=1}^{N}\left[\langle x\rangle - x_i\right]\cdot\left[\langle y\rangle - y_i\right]}{S_x \cdot S_y} \qquad (11)$$

RESULTS AND DISCUSSION

The structures of slug flows have been identified at the four measuring stations for various flow rates. For each mixer type were conducted nine experimental runs at the same pair of air and water superficial velocities, as identified in Table 1. The water and the air superficial velocities spanned from 0.25 m/s to 1.33 m/s, and 0.33 Sm/s to 1.67 Sm/s, respectively. The number of unit cells indicates the size of the sample in terms of valid unit cells, which passed through the sensors during the acquisition period. For convenience is also shown in Table 1, the mixture pipe Reynolds number, the Froude number numbers are defined as:

$$Re = \frac{J \cdot d}{\nu_L} \text{ and } Fr = \frac{J}{\sqrt{gd}} \qquad (12)$$

where J = JL+JG and J is the mixture superficial velocity, ν and ρ represent the water kinematic viscosity and density, respectively and d is the pipe diameter.

A photographic record of the bubble tail and nose is shown in Fig. 5 for runs #1, #2, #3, #5, #6 and #7. The photographs come from frozen frames of a black and white high-speed digital movie recorded at 494 diameters downstream of the concentric mixer, station S3. Each test section captured in each frame has a view of approximately four pipe diameters along the streamwise direction. To help identify the interface a hand drawn line is superposed on the actual picture. It enhances the contours of the bubble tail and nose shapes. As additional information, all frames show two straight and vertical bright lines. They are the twin parallel gold wires stretched across the pipe section with 50 mm apart from each other. For run #1, is observed a well-defined bubble nose with a stable shape attached to the pipe top wall. An increase on the gas flow rate, as occurs from run #1 to #3, causes the bubble nose to bend toward the pipe center in an irregular shape with a not stable interface. The bubble tail has always an angle greater than ninety degrees with respect to the base liquid film. For the present runs, the bubble tail has dispersed bubbles for air to water flow ratio greater than unit. Runs #1 and #5 have negligible air content within the liquid slug. The length of the aerated volume on the liquid slug is within 1 to 4 pipe diameters, with the exception of #8 and #9.

Table 1. Superficial velocities, number of unit cells, acquisition period, Reynolds, Froude numbers for each run.

Run #	JG (Sm/s)	JL (m/s)	# Cells (---)	Period (s)	Re (x 10^4)	Fr
1	0.33	0.67	350	600	2.7	2.0
2	0.33	1.33	360	600	1.3	3.3
3	0.33	1.67	320	600	5.0	4.0
4	0.50	0.50	470	360	2.6	2.0
5	0.67	0.67	700	360	3.3	2.7
6	0.67	1.33	550	360	5.0	4.0
7	0.67	1.67	500	360	6.0	4.7
8	1.33	0.67	1600	240	5.0	4.0
9	1.33	1.33	1400	240	6.5	5.3

The velocity of the elongated bubble

Most of the transported gas is carried within the elongated bubble. An accurate prediction of the gas flow rate needs detailed knowledge on the bubble shape and its velocity. The present section deals with the nose velocity of the elongated bubble in a presence of a train of slug units.

Regarding this matter, several theoretical and experimental studies were performed. Based on experiments with an isolated bubble Nicklin et al (1962) proposed a linear "drift-flux like" relationship to determine the bubble nose velocity,

$$VB = C_0 \cdot J + V_\infty \qquad (13)$$

where the constants C_0 and V_∞ are associated, in order, to the phase's distribution and to the bubble drift velocity in a fluid at rest.

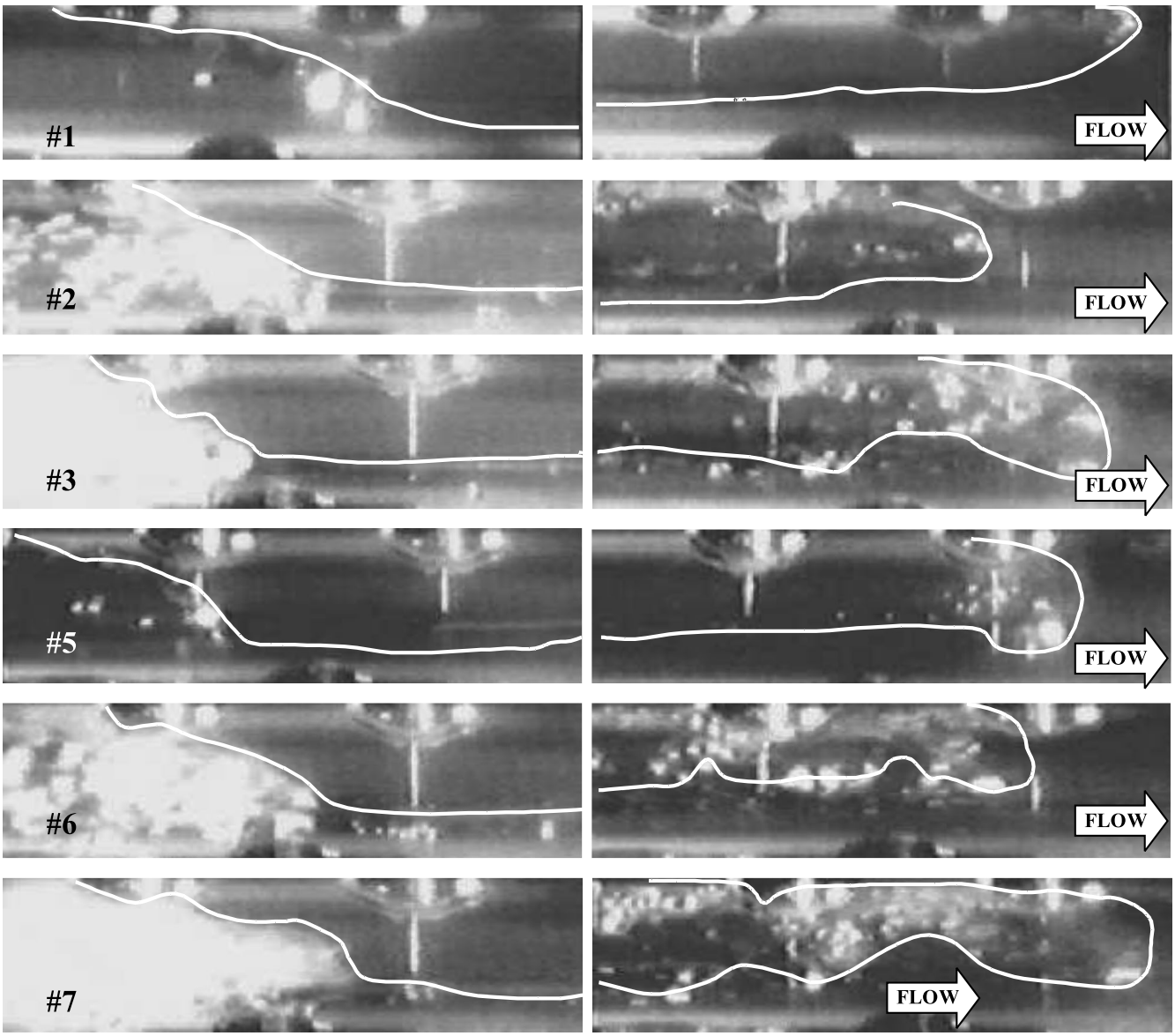

Figure 5. Photographs of the slug front and bubble tail for runs #1, #2, #3, #5, #6 and #7.

The constants C_0 and V_∞ are in fact dependent on several parameters such as pipe diameter, pipe inclination angle, mixture velocity, surface tension and liquid viscosity among others Fabre and Liné (1992). It is not straightforward to extend the behavior of a single bubble to a train of bubbles. The bubble motion is influenced by the interactions among the neighboring cells. Nevertheless, the insight gained by the theoretical and experimental analysis of single bubble experiments sheds light on the experimental analysis of a train of bubbles. The idea behind the relationship proposed by Nicklin is put forward on train of bubbles as the bubble velocity is composed by superposition of the mixture velocity and the drift velocity. According to Bendiksen (1984), the coefficients C_0 and V_∞ for horizontal flows are usually chosen as:

$$C_0 = 1.0 \text{ and } V_\infty = 0.54 \text{ if } Fr < 3.5$$
$$C_0 = 1.2 \text{ and } V_\infty = 0.00 \text{ if } Fr \geq 3.5 \quad (14)$$

For regimes where the Fr less than 3.5 there exists a gravity-induced drift resulting from the elevation difference in the bubble nose, Benjamin and Broke (1968). For Froude values greater than 3.5 the inertia force overcome the gravity force and the drift velocity on the horizontal slug flow is zero.

A direct comparison between the experimental determined coefficients and the accepted Bendiksen values, Eq. (8) is drawn. The experimental averaged bubble velocity is presented against the mixture velocity in Fig. 6.

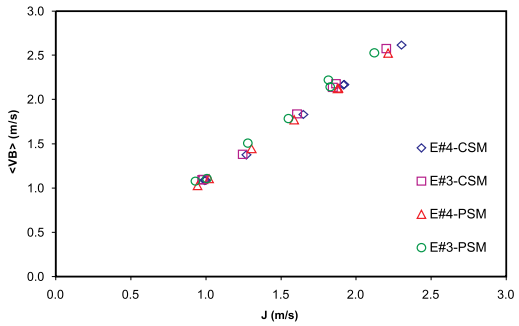

Figure 6. Averaged bubble nose velocity against mixture velocity. Data for measuring stations S3 and S4 for CSM and PSM mixers.

The data come from the experiments using the concentric and parallel stream mixers. The sample size of each run is in Table 1. The sample size, the data repeatability and linearity, and also the flow measurement accuracy and the horizontal alignment of the pipeline rack, are favorable indicators of the data consistency. The bubble nose velocity is for stations S3 and S4 where the entrance effects are fading away. The experimental values of the constants C_0 and V_∞ result of a least square fit displayed on Table 2. The data belonging to each station fits remarkably well by the linear relation of Eq. (7) exhibiting a R squared value of 0.99 or greater. It is observed a mild decrease of C_0 considering the distance from the mixer while V_∞ is zero through out the stations S3 and S4. The influence of the formation mechanism implied by the use of different mixers on C_0 and V_∞ is not observed at distances of 494D and 777D from the gas-liquid mixer. In fact C_0 changes are less than 2% for both cases while V_∞ does not change at all.

The experimental data of C_0 is of 1.12 laying between 1.0 and 1.2 as suggested by Eq. (14) but it does not show any dependence with the Froude number as suggested.

Table 2. The C_0 and V_∞ constants from a least square fit of the experimental data.

	Station	C_0	V_∞ (m/s)	R^2
Concentric Stream Mixer	S3	1.15	0	0.996
	S4	1.12	0	0.997
Parallel Stream Mixer	S3	1.18	0	0.992
	S4	1.12	0	0.998

Bubble interactions

The interactions between the the neighboring bubbles are one of the factors responsible to the flow non-uniformities in time and space. They cause changes in the speed, which result in changes on the lengths that may end up in bubble coalescence if two consecutive bubbles touch each other. When two bubbles merge to a single one the length of the bubble increase, the volume of liquid slug between then is displaced to the neighboring slugs and the unit period changes. The interactions between the gas and liquid structures are higher at the flow entrance exhibiting a high coalescence rate Rosa et al.(2001 a-b). Increasing the distance from the mixer, the coalescence rate decreases exponentially, the average quantities such as sizes and velocities change slowly but the intermittent behavior still exists. Duckler et al. (1985) uses this slow change properties region to establish a minimum stable slug length where the influence on the trailing bubble is negligible. They argue about the minimum slug length necessary to establish a fully developed velocity profile ahead of the trailing bubble. Moissis and Grifth (1962), prior to Duckler, proposed a kinematic dependence on the trailing bubble velocity with the liquid slug length ahead of it. The original relationship was developed based on the interactions of two isolated bubbles flowing in ascendant vertical direction. They found that the trailing bubble velocity is a function of the separation distance between bubbles, and fitted the experimental data using a exponential decay law with the distance:

$$\frac{VB_T}{VB_L} = 1 + 8\exp\left(-1.06 \cdot \frac{LS}{D}\right) \qquad (15)$$

where the subscripts T and L stands for trailing and leading bubble velocity. Barnea and Taitel (1993) used a similar relation with different coefficients for the horizontal case. More recently, Fagundes (1999) further improved the kinematic relation for horizontal flow but still based his results on two bubbles interaction.

The present work investigates experimentally this general kinematic law in a presence of a train of bubbles. The data used on this analysis belongs to station S4, 777D downstream the mixer. Three interaction mechanisms are investigated in terms of correlation coefficients, they are: a) a relationship between the leading and trailing bubble velocities, b) a dependence of the bubble velocity on the length of the liquid slug ahead of it, and c) the dependence of the logarithm of the leading bubble to the trailing bubble velocity ratio on the slug length between them. The first and the second investigated mechanisms are quite straightforward: they seek if the trailing bubble velocity increases if it comes after a faster bubble or a lengthier slug. The third one seek some type of kinematic mechanism proposed in Eq. (15).

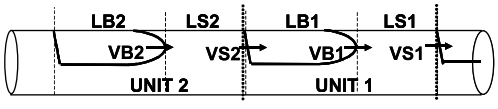

Figure 7. Nomenclature for the neighbor unit cells

The degree of the linear relationship between the variables involved on the studied cases (a), (b) and (c) is determined by the correlation coefficient. Figure 7 portraits the variables involved on the evaluation of the correlation coefficients. The labeling identifies two consecutive units and associates the indexes (1) and (2) to the leading and to the trailing units. For convenience the correlation coefficients of the proposed mechanisms (a), (b) and (c) are identified as R(a), R(b) and R(c) and defined in Eqs. (16), (17) and (18).

Scatters plot of the variables involved in mechanisms (b), (c) are shown in Fig. 8 for run #4 with data taken from station S4 using a PSM mixer. Figure 8(a) shows the bubble velocity against the liquid slug length ahead of it. Figure 8(b) has the logarithm of the leading bubble to trailing bubble velocity ratio against the slug length between them. As seen from Fig. 8, cases (b) and (c) do not display any clear trend between the chosen variables.

Table 3 shows the linear regression coefficients for mechanisms in cases (a), (b) and (c). The data is taken from station S4 for runs #1 to #9 using the Parallel Stream Mixer. Neither one of the three studied mechanisms proved to show a good linear relationship. The increase on the leading bubble velocity does not imply an increase on the trailing bubble velocity, its linear regression coefficient, R(a) stayed always less than 0.1. Also the length of the liquid slug does not directly affects the speed of the trailing bubble, R(b) was always less than 0.21. Finally the induced velocity of the leading bubble to the trailing bubble was not dependent from the distance between bubbles, R(c) was not greater than 0.12.

$$R_{(a)} = \frac{\sum_{i=1}^{N}\left[\langle VBl\rangle - VBl_i\right]\cdot\left[\langle VB2\rangle - VB2_i\right]}{(N-1)\cdot S_{VBl}\cdot S_{VB2}} \quad (16)$$

$$R_{(b)} = \frac{\sum_{i=1}^{N}\left[\langle VBl\rangle - VBl_i\right]\cdot\left[\langle LSl\rangle - LSl_i\right]}{(N-1\cdot)S_{VBl}\cdot S_{LSl}} \quad (17)$$

$$R_{(c)} = \frac{\sum_{i=1}^{N}\left[\left\langle Ln\left(\frac{VB2}{VBl}\right)\right\rangle - Ln\left(\frac{VB2}{VBl}\right)_i\right]\cdot\left[\langle LS2\rangle - LS2_i\right]}{(N-1)\cdot S_{Ln(VB2/VB1)}\cdot S_{LSl}} \quad (18)$$

The experimental data taken in a sequence of bubbles shows that the velocities between neighboring gas bubbles are not solely represented by kinematic laws described in two-bubble experiments but it might be defined by other kinematic and dynamic mechanisms still to be revealed.

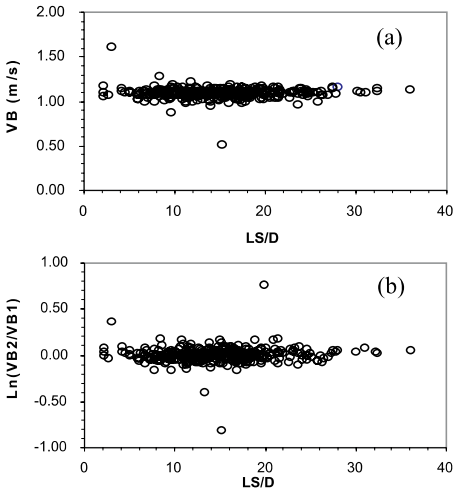

Figure 8. Scatter plots for bubble to bubble interaction mechanisms (b) and (c) for taken at station S4 using PSM mixer for run #4.

Entrance mechanism

The statistical populations of sizes, velocities and frequencies belonging to the bubbles and slugs far from the inlet results from the way slugs are created at the inlet and also by the way they interact as they travel along the pipe. If no interaction happens, the gas and the liquid structures keep memory of the entrance through out the pipe. On the contrary, if the space interaction between bubbles is strong the flow may attain a fully developed state with stationary statistical populations independent of the entrance mechanisms. The assessment of the effects of the entrance mechanisms and of the bubble to bubble interactions is now pursued comparing the probability density functions of the bubble velocities at the nearest and farthest measuring positions, i.e. stations S1 and S4.

Table 3. Correlation coefficients R(a), R(b) and R(c) taken at station S4, using PSM mixer, for runs #1 to #9.

Correlation	R(a)	R(b)	R(c)
Run			
#1	-0.02	+0.21	+0.12
#2	-0.02	-0.08	-0.04
#3	-0.05	+0.03	-0.02
#4	+0.01	+0.04	-0.03
#5	+0.09	+0.12	+0.08
#6	-0.01	+0.05	+0.01
#7	-0.08	-0.01	-0.07
#8	-0.01	-0.01	-0.07
#9	+0.01	+0.04	+0.05

This task was accomplished experimentally generating slug flow by means of different entrance mechanism. The two types of mixers are the concentric stream mixer, CSM, and the parallel stream mixer, PSM. The CSM mixer issues a concentric air jet surrounded by water flowing on the annular space. The air jet is broken into small bubbles, which are quickly carried by the water stream. Owing to the buoyancy force, the bubbles migrate to the top of the pipe, coalesce, form large bubbles surrounded by liquid pistons that evolve to the known slug flow pattern. The PSM uses an internal plate to divide the pipe cross-section into two co-current parallel streams: the water stream flows on the bottom channel and air on the top channel. The mixer is about 10 pipe diameters long. After this distance the water and air streams are put together. A Kelvin Helmoltz type instability develops along the air-water interface. The interface waves grow and eventually block the pipe cross section, and ends up establishing the slug flow pattern.

Experimental data relative to the instantaneous bubble front velocities, VB for runs #1 and #6, are taken at 127D and 777D (the first and fourth measuring stations) using the CSM and the PSM mixers. The chosen runs have the same gas-liquid ratio of 2 but run#1 has a mixture velocity of 100 cm/s while the run#6 has one of 200 cm/s. The data is further processed to give rise to histograms of VB shown in Figs. 9 and 10, respectively.

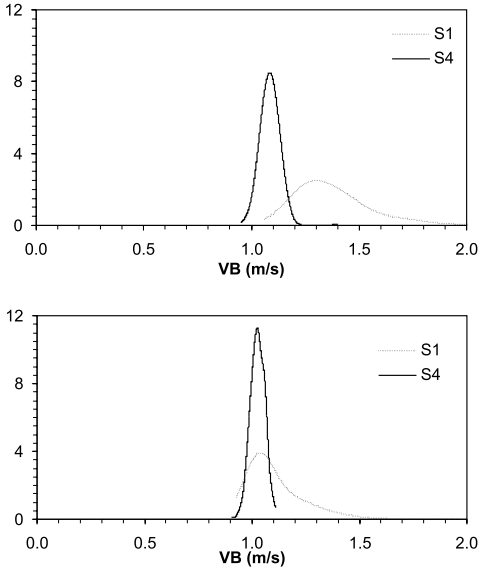

Figure 9. VB histograms for run#1 generated by CSM mixer (top) and PSM mixer (bottom).

Considering Fig. 9 at station S1, where the entrance effects are dominant, the VB distributions are quite distinct from the one at S4. The area blockage of the air injector causes the CSM mixer to produce bubbles with a higher mean velocity than the PSM mixer. Due to the occurrence of small bubbles during the slug formation, the CSM mixer generates VB with a large standard deviation when compared against the PSM mixer. As the flow evolves to station S4 the changes on the population are minor, the flow becomes more ´organized´ in a sense that the VB samples have smaller standard deviation. Also the similarities between the CSM and PSM samples start arising due to the similarities among the histograms. This is an indication that the entrance effects are fading away, but even at 777 D downstream the mixer small differences on the samples frequencies are still detected.

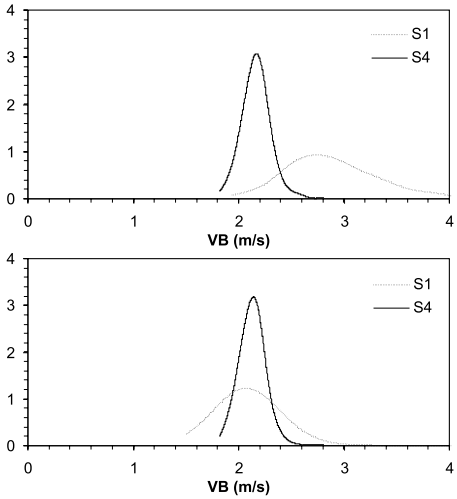

Figure 10. VB histograms for run#6 generated by CSM mixer (top) and PSM mixer (bottom).

Figure 10 depicts the histograms for run#6. The overall behavior of the histograms is the same of run#1. The exception for run#6 is that the VB histograms at S4 for CSM and PSM mixers are identical. This indicates that the flow entrance mechanisms have no effect at 777 D downstream the mixer. The population exhibits the same mean and standard deviation.

The VB histograms in Figs. 9 and 10 also portraits information related to the bubble to bubble interaction. The bubble velocity population at 127D, although dependent of the mixer type, has a mean and standard deviation greater than the ones observed at 777D. As the bubble velocity population evolves from station S1 to S4 the high and the low speed bubble occurring in S1 disappears. The resulting velocity population in S4 has minimum and maximum velocity values much less than the ones observed in S1. This reduction is due to the bubble to bubble interaction. The faster bubbles overtake the slow ones in a process known as coalescence. It clearly indicates that the coalescence process requires bubbles traveling at different speeds. Once the kinematic mechanisms can not by themselves justify the trailing bubble velocity acceleration due to the wake effect of the leading bubble, the differences in speed may be associated right at the bubble formation.

That is, the bubble creation process imparts different bubble speeds resulting in VB populations at 127D as seen in Figs. 9 and 10. The bubbles, created with high and low speed travels along the pipe and eventually one high speed overtakes a low speed bubble. The bubble velocity differences due to the creation process may overshadow the kinematic law observed in a two-bubble experiments. This idea is still to be proved and currently is under investigation.

CONCLUSIONS

Still photographs show a change on the bubble shape as the velocity increases. For low speed regime the bubble has a well defined nose and tail. As the fluid velocity increases the gas-liquid interface becames disturbed by waves, the nose points toward the center of the pipe and the tail is highly aerated, as shown on Fig. 5. The mean velocity of the bubble nose has a linear dependence with the mixture superficial velocity. The dependence with the Froude number on C_0 and V_∞ was not found. The constant C_0 is 1.12 for both mixers. The drift velocity, V_∞ was not detected for the range of Reynolds and Froude numbers of the experiments. The bubble to bubble interactions was pursued by means of a search of linear regression coefficients choosing three mechanisms. None of them exhibited a definite linear regression coefficient. The experimental data taken in a sequence of bubbles shows that the velocities between neighboring gas bubbles are not solely represented by kinematic laws described in two-bubble experiments but it might be defined by other kinematic and dynamic mechanisms still to be revealed. Finally, it was observed that the entrance effects fade away after a downstream distance from the mixer. The resulting distributions of VB are found the same despite of being generated by different entrance mechanisms.

ACKNOWLEDGEMENTS

This work was funded by the PETROBRAS and FINEP-CTPETRO projects n. 65.2000.0043.00 and n. 2101034100, respectively.

REFERENCES

Andreussi, P. and Bendiksen, K., 1989, An investigation of void fraction in liquid slugs for horizontal and inclined gas-liquid pipe flow, Int. J. Multiphase Flow, Vol15, pp. 937-946.

Benjamin, T. Brooke, 1968, Gravity Currents and Related Phenomena, J. Fluid Mech., Vol.31, part 2, pp. 209-248.

Barnea, D. and Brauner, N., 1985, Holdup of the liquid flow in two-phase intermittent flow, Int. J. Multiphase Flow, Vol 11, pp. 43-49.

Barnea, D. and Taitel, Y, 1993, A model for length distribution in gas-liquid flow, Int. J. Multiphase Flow, Vol 19, pp. 829-837.

Bendiksen, K.H., 1984, An Experimental Investigation of the Motion of Long Bubbles in Inclined Tubes, Int. J. Multiphase Flow, Vol 10, n. 4, pp. 467-483.

Crowe, C., Sommerfeld and M. and Tsuji, Y., 1998, *Multiphase Flows with Droplets and Particles*, CRC Press, 471 p.

Dukler, E. and Hubbard, M.G., 1975, A model for gas-liquid slug flow in horizontal and near horizontal tubes, Ind. Eng. Chem. Fundam., Vol 14, n.4, pp.377-347.

Dukler, E., Maron, D.M. and Brauner, N., 1985, A physical model for predicting the minimum stable slug length. Chem. Eng. Sci., 40: 1379-86.

Fabre, J. and Liné, A., 1992, Modeling of two-phase slug flow, Annual Review of Fluid Mech., 24:21-46.

Fagundes Netto, J.R, 1999, Dynamique de Poches de Gaz Isoléesen écoulement Permanent et Non-permanent Horizontal, Ph.D. thesis, Institut National Polytechnique de Toulouse, France.

Grenier, P., 1997, Evolution des longuers de bouchons écoulement intermittent horizontal, Ph.D thesis, Institut National Polytechnique de Toulouse, France.

Moissis, R. and Griffith, P., 1962, Entrance effects in a two-phase slug flow, J. Heat Transfer, pp. 29-39.

Nicklin, D.J., Wilkes, J. and Davidson, J.F., 1962, Two-phase Flow in Vertical Tubs, Trans. Inst. Chem. Engng, Vol.40, pp61-68.

Nydal, O.J., Pintus, S. and Andreussi, P., 1992, Statistical characterization of slug flow in horizontal pipes, Int. J. Multiphase Flow, 18,3,pp. 439-453.

Rosa, E.S.; Morales, E.R; Melo, A.I., Freire, R. and França, F.A., 2001a, The Evolution of Horizontal Slug Flow, XVI Congresso Brasileiro Eng. Mecânica, COBEM, Uberlândia, 26 a 30 de Nov., pp. 1 a10, CD ROM.

Rosa, E.S., Morales, E.R., Melo, A.I.; Freire, R.C. and França, F.A. ; The Slug Flow Evolution in a Horizontal Pipeline, Canadian International Petroleum Conference, 2001b Calgary, Alberta – Canada, June 12-14, paper 2001-176, 14 pages.